Journal of Power Sources 644 (2025) 237167

Contents lists available at ScienceDirect

Journal of Power Sources

journal homepage: www.elsevier.com/locate/jpowsour

An accelerated aging test procedure for lithium-ion battery based on a dual-temperature approach

Simone Barcellona [a,*], Silvia Colnago [b], Lorenzo Codecasa [a], Luigi Piegari [a]

[a] Department of Electronics, Information and Bioengineering, Politecnico di Milano, Italy
[b] Department of Generation Technologies and Material, Ricerca sul Sistema Energetico S.p.A., Milan, Italy

HIGHLIGHTS

- Accelerated cycle aging test on lithium cobalt oxide batteries.
- Dual-temperature method balances SEI growth and lithium plating stress.
- Achieved over 5 × acceleration without altering aging mechanisms.
- Validated by comparison with a non-accelerated test on the same battery.

ARTICLE INFO

Keywords:
Lithium-ion battery
Accelerated cycle aging procedure
Capacity fade

ABSTRACT

Lithium-ion batteries (LiBs) are essential for diverse applications, but their degradation—driven by aging mechanisms such as solid electrolyte interface (SEI) formation, lithium plating, and electrode particle cracking—limits their performance and lifespan. These mechanisms result in degradation modes such as lithium inventory loss and active material depletion. Understanding these processes requires extensive aging tests, which are time-consuming and costly. Accelerated aging tests aim to expedite this process while preserving the same aging mechanisms observed under normal conditions. Among stress factors, temperature is widely used, as higher temperatures accelerate SEI growth, while lower temperatures promote lithium plating. However, conventional accelerated tests often achieve limited acceleration or unintentionally alter aging mechanisms. To address this, we propose a novel accelerated cycle aging procedure using dual-temperature conditions—charging at 20 °C and discharging at 40 °C. This approach balances SEI growth and lithium plating stress, replicating normal aging at 25 °C while achieving an acceleration factor of more than 5 or even 8. The method was validated through experiments comparing the proposed test with a reference non-accelerated aging test on identical batteries. The results suggest that this approach effectively preserves aging mechanisms, offering a reliable and efficient pathway for battery aging studies.

1. Introduction

Among energy storage systems, lithium-ion batteries (LiBs) are the most widely used in manifold applications. Thanks to their high energy density, high power density, high efficiency, low self-discharge, and lack of memory effects, they represent a highly promising storage solution for both stationary and mobile applications. Furthermore, climate change, the shortage of fossil fuels, and concerns regarding environmental pollution are driving the transition toward green energy and sustainable mobility. As a result, LiBs are widely used as storage systems integrated with renewable energy sources or as power sources in various mobile devices, ranging from small electronics such as laptop, smartphones, and medical tools to larger applications such as electric vehicles [1].

LiBs come in various compositions, depending on the type of electrodes and electrolytes. In particular, their anodes are mostly carbon/graphite-based, though materials such as lithium titanate oxide (LTO) and silicon-based materials are also used [2]. Cathode materials vary, including lithium iron phosphate (LFP) and several lithium metal oxides such as lithium cobalt oxide (LCO), lithium manganese oxide (LMO), lithium nickel manganese cobalt oxide (NMC), and lithium nickel cobalt aluminum oxide (NCA). Typically, LiBs with carbon/graphite-based anodes are named according to their cathode material. The electrolyte

* Corresponding author.
E-mail address: simone.barcellona@polimi.it (S. Barcellona).

https://doi.org/10.1016/j.jpowsour.2025.237167
Received 9 December 2024; Received in revised form 18 April 2025; Accepted 22 April 2025
Available online 27 April 2025

used in LiBs consists of an inorganic lithium salt dissolved in organic carbonate-based solvents. Often, $LiPF_6$ serves as the solute, while the solvent is a blend of ethylene carbonate, dimethyl carbonate, diethyl carbonate, and methyl ethyl carbonate in various ratios [3]. Ongoing research aims to explore alternative materials and combinations for electrodes and electrolytes to enhance battery performance further [4,5]. Additionally, LiBs are available in different shapes and sizes, each with distinct advantages and drawbacks in terms of energy density, power density, lifespan, safety, and cost. The selection of a specific LiB type depends on its intended application and operating conditions.

Focusing on LiBs with carbon/graphite-based anodes, these batteries undergo various aging mechanisms, such as solid electrolyte interface (SEI) growth, lithium plating, metal dissolution, gas evolution, electrode particle cracking, current collector corrosion, and electrolyte decomposition. These processes can occur when LiBs are not used, based on storage conditions (calendar aging), and/or when they are operating, based on the working conditions (cycle aging). Such aging mechanisms result in degradation modes such as loss of lithium inventory (LLI), loss of active materials (LAM), loss of electrolyte (LE), and conductivity loss (CL) [6]. These aging mechanisms and modes are illustrated in Fig. 1.

LLI refers to the depletion of active lithium available for intercalation/deintercalation chemical reactions and encompasses various processes, including the formation, growth, cracking, and reformation of the SEI. In the early stages of the lifecycle of a LiB, the establishment of a stable SEI leads to significant LLI, which gradually diminishes over time. Lithium plating, which refers to the deposition of metallic lithium on the surface of the anode of LiBs during charging, especially at low temperatures, is another important aging mechanism leading to LLI [7]. Actually, from a theoretical standpoint, lithium plating is a reversible process. Specifically, some plated lithium can be re-intercalated into the anode during the constant voltage phase or relaxation time, while some may dissolve during discharge, releasing extra lithium ions in a process known as lithium stripping [8]. However, it is important to note that a portion of the plated lithium may undergo other chemical reactions with the electrolyte, contributing to the formation of additional SEI, or lose electrical contact with the anode, which results in what is commonly referred to as dead lithium.

LAM is related to the loss of electrode particles that can host lithium and is attributed to different aging mechanisms, including metal dissolution, electrode particle cracking, and graphite exfoliation. LE and CL are two degradation modes that occur alongside LLI and LAM. In fact, SEI formation and graphite exfoliation consume electrolyte, contributing to LE, while CL, which is related to the loss of conductivity, arises from LE, current collector corrosion, or binder decomposition.

Consequently, LiBs experience a reduction in the total energy they can store (capacity fade) and the maximum power they can deliver (power fade) [9]. For this reason, in the literature, the state of health (SOH) of a battery is typically assessed using one of these two indicators. Specifically, capacity fade is primarily caused by the decrease in available lithium ions, i.e., LLI. Additionally, LAM can contribute to capacity fade due to the delocalization of lithium ions [10]. Power fade, on the other hand, is mainly attributed to CL. Finally, LE contributes to both capacity and power fade by reducing the number of lithium ions and compromising the electrolyte's ability to effectively wet or penetrate the porous structure of the electrodes.

Battery degradation can be reduced, and its efficiency and lifespan increased through two main approaches: enhancing its chemical and physical construction and ensuring that LiBs operate under optimal conditions. In fact, battery aging mechanisms and degradation modes can be either accelerated or slowed by various stress factors, such as temperature, state of charge (SOC), voltage limits, and current rate. However, understanding which factors have the most significant impact and how they affect battery degradation is still debated, often leading to discordant results. This can be due to the different chemistries of LiBs or the lack of clearly defined test conditions. Nevertheless, there are some common and validated results in the literature.

Particularly for calendar aging, it is well established that it mainly depends on the SOC and temperature at which LiBs are stored, and that, within certain limits, higher temperatures generally lead to faster degradation according to the Arrhenius law [11]. In fact, as mentioned in Ref. [12], storage temperatures exceeding 65 °C can trigger other aging mechanisms, deviating from the exponential behavior predicted by the Arrhenius law. The SOC dependency is slightly different, as it depends on the materials composing the electrodes. In any case, for most LiBs, higher SOCs result in faster degradation [13].

On the other hand, understanding how cycle aging affects LiB degradation is more challenging, and in some cases, the results are contradictory. Nevertheless, many researchers agree that cycle aging depends on factors such as the cycling SOC range, temperature, operating voltage limits, and current rates. Different or even opposite results can be found, particularly regarding the cycling SOC range and current rate. Regarding the cycling SOC range, there are some works [14–20] in the literature that examined its impact on the cycle aging of LiBs, yielding conflicting findings. In Refs. [14,15], researchers cycled different NMC batteries across various SOC ranges at consistent temperature and current rates, revealing that batteries aged more rapidly at higher SOC ranges for the same number of cycles. Similar conclusions were drawn in Ref. [16] for LMO/NMC batteries and in Refs. [20,21] for LCO batteries. Conversely, studies in Ref. [17] for LMO/NMC batteries and [18] for NMC batteries demonstrated that, under identical temperature and current rate conditions, batteries aged more quickly at both low and high SOC ranges, with minimal degradation observed when the battery was cycled around 50 % of SOC. On the contrary, in Ref. [19], it was demonstrated that for NCA batteries, the aging rate became faster as

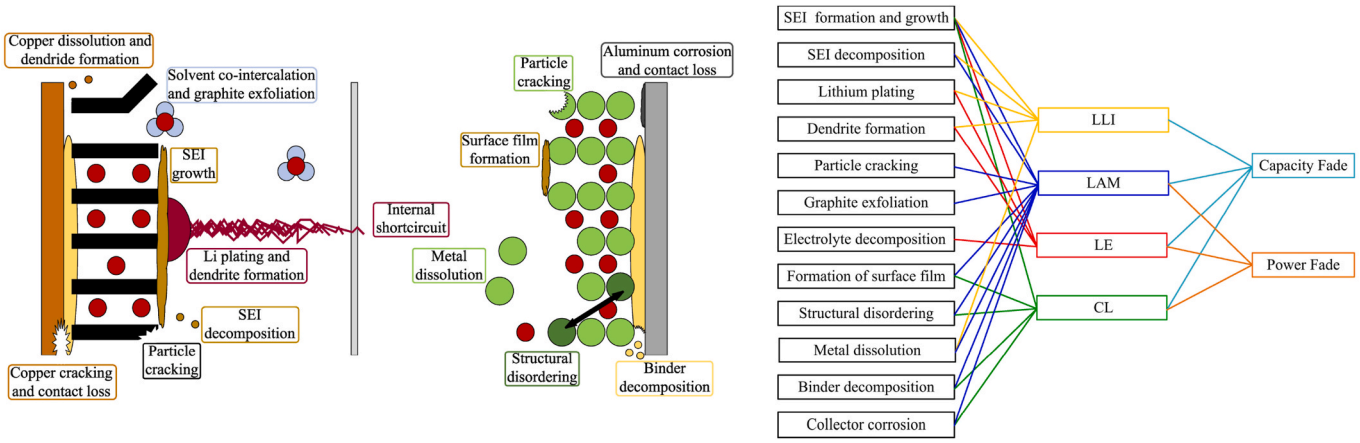

Fig. 1. Main aging mechanisms and aging modes.

the SOC regions shifted towards higher values, reaching its peak in the medium/high SOC ranges (65–85 % of SOC). However, beyond this threshold, the aging rate declined once more. Regarding the current rate, in Ref. [22], the authors found that for LCO batteries, the capacity fade at different discharge current rates was the same as a function of the number of cycles. Similarly, in Ref. [23], the authors demonstrated that LCO batteries, under symmetrical charging/discharging cycles at different current rates, showed the same capacity fade as a function of the total moved charge. Conversely, in Refs. [24–26], for LCO and LFP batteries respectively, significant effects of the current rate on battery aging were reported. On the other hand, researchers agree with the general trend of how temperature affects cycle aging, which is consistent even for different battery chemistries [27,28]. This trend usually follows the well-known V-shaped Arrhenius behavior in terms of the aging rate, which identifies the temperature where the aging rate is minimized [11]. This temperature, which is considered the crossover point between the two dominant aging mechanisms, namely SEI growth and lithium plating, can change with battery chemistry and current rates. However, for most LiBs cycled at medium current rates, this temperature is around 25 °C [11,29]. Specifically, for temperatures typically higher than 25 °C, the aging trend follows an Arrhenius like-behavior, where the rate of aging increases as the temperature rises, mainly attributed to SEI growth [12,30–33]. Like for calendar aging, this is only true within specific temperature intervals. When cycling the battery at elevated temperatures, the aging mechanisms become more complex due to increased heat generation [6]. Furthermore, when temperatures exceed a certain threshold, additional heat generation may occur, potentially leading to thermal runaway [34]. In contrast, for temperatures lower than about 25 °C, the aging rate follows the reverse trend of the Arrhenius like-behavior, with higher degradation for lower temperatures, mainly due to lithium plating.

In light of the above, the study of battery aging is currently highly challenging and deeply investigated. The main issue lies in the paradoxical nature of aging analysis itself. While LiBs are designed to last as long as possible, analyzing their aging requires a significant amount of time to reach predetermined degradation conditions. Therefore, well-established accelerated aging tests are being investigated to speed up the aging process while ensuring that the primary aging mechanisms under study remain unaltered [6,35]. The acceleration is typically achieved by exposing LiBs to more severe operating conditions than those encountered during regular use, with the aim of determining the threshold values of stress factors at which the dominant aging mechanisms undergo significant changes. The results obtained from these tests could facilitate the development of analytical models that align with capacity or power fade curves within predefined stress factor ranges, thereby contributing to the creation of an accelerated aging-based lifetime prediction model. It is worth highlighting that the concept behind accelerated aging tests is based on the observation that certain aging mechanisms in LiBs stem from similar underlying physicochemical phenomena, which establish relationships with associated stress factors at the microscopic level. Therefore, within stress factor ranges where the dominant aging mechanisms remain largely unchanged, the proposed aging test procedure should ensure that the aging mechanisms experienced by LiBs are consistent under both non-accelerated and accelerated conditions. On one hand, this approach allows the derivation of a reliable lifetime prediction model. On the other hand, from a physicochemical standpoint, the evolution of battery degradation under accelerated conditions can be considered to follow the same trend as under non-accelerated conditions.

These accelerated aging tests are typically performed by subjecting the battery to thermal, electrical, or mechanical stresses [6,35–37]. Thermal stress involves varying the ambient temperature or directly cooling or heating the battery while it is stored or in operation. Electrical stress generally includes storing the LiB at different SOC levels or cycling it within different voltage or SOC ranges and current rates. Mechanical stress exposes LiBs to various forces and vibrations. In any case, commonly used accelerated stress factors include battery temperature, charging/discharging current rates, voltage limits, and SOC levels/ranges. During these tests, various aging mechanisms should be analyzed. Typically, this analysis can be conducted through electrical characterization or post-mortem analysis [6,38].

In the present work, the focus is on temperature, which, among the stress factors for both calendar and cycle aging, stands out as a critical factor impacting battery lifespan. Both elevated and reduced temperatures accelerate battery degradation through different aging mechanisms. Therefore, the use of temperature as a stress factor must be carefully managed to prevent multiple aging mechanisms concur. First, it is essential to determine the dominant aging mechanism to be analyzed. Once identified, the appropriate application of the stress factor can be assessed. In the next section, a literature review on the effect of temperature in accelerating battery aging is presented and compared.

Based on the results, this study introduces a novel accelerated cycle aging test procedure, applied to LCO battery chemistry, that charges and discharges the battery at two different temperatures to expedite battery degradation in terms of capacity fade, along with a related analytical model. Specifically, by charging the battery at a low temperature and discharging at a higher temperature, the two main aging mechanisms—SEI growth and lithium plating—can be stressed in a balanced manner. This approach replicates normal aging tests performed at the reference room temperature of 25 °C and can potentially achieve an acceleration factor exceeding 5 without altering the aging mechanisms compared to normal operating conditions. Finally, the proposed accelerated cycle aging test was experimentally validated by comparing its results with those of a reference non-accelerated cycle aging test conducted on the same battery type.

Although the proposed accelerated cycle aging test procedure was conducted on a specific battery chemistry, LCO, future research could explore its applicability to other chemistries to determine whether the procedure can be extended.

2. Temperature effect on battery aging

In the literature, many studies used temperatures higher than room temperature (20–25 °C) to accelerate aging tests and develop models that are suitable for room temperature conditions. These models aim to predict SEI growth, which, as previously mentioned, is the dominant aging mechanism for most LiBs within the temperature range of approximately 20–25 °C–40 °C. In fact, only slightly elevated temperatures merely expedite the SEI growth process without introducing any other dominant mechanisms. The SEI is empirically found to growth as a function of the square root of time or the number of cycles [31,39–41]. The SEI is of paramount importance in stabilizing the battery and preventing further LLI and LE. Specifically, during the first cycles, SEI formation is rapid, leading to the depletion of around 10 % of the active lithium and increased battery resistance. Subsequently, as the battery undergoes further cycles, although the process occurs gradually, the electrolyte and active lithium continue to be consumed, resulting in the thickening of the SEI layer. This constitutes the primary mechanism behind the long-term aging of LIBs.

With rising temperatures, other side chemical reactions may emerge, leading to a change in the composition of the SEI. In this regard, many research works indicate that at elevated temperatures, the quantity of inorganic salts diminishes while organic content increases, thereby reducing the protection provided by the SEI on electrode active materials [42]. Moreover, at high temperatures, the electrolyte accelerates its decomposition, and gas generation increases as well. Consequently, battery expansion can occur, and the contact between current collectors and electrodes may weaken. This ultimately results in a significant increase in internal resistance [43]. Finally, at elevated temperature, cycle aging can also lead to particle cracking in the graphite electrode and dissolution of metal in electrodes [44]. Therefore, all these phenomena

contribute to a faster decline in battery performance, leading to a distinct point on the capacity fade curve. This point, known as the knee-point, marks the transition between low and high aging rates [45]. In light of the above, it is possible to claim that SEI growth is the primary factor behind the linear aging behavior in a moderate temperature range, as supported by many authors [17,46–50].

At low temperatures, lithium-ion diffusion slows down, along with the intercalation/deintercalation reactions, which leads to lithium deposition (lithium plating) on the anode electrode made of carbon-based materials, particularly during fast charging [34,35]. The increased battery resistance contributes to the gradual buildup of lithium deposition on the negative electrode surface, which can lead to the formation of dendrites. These dendrites can eventually detach, becoming inactive lithium (dead lithium), causing irreversible LLI. Additionally, these dendrites can penetrate the separator, resulting in internal short circuits. It is commonly recognized that lithium plating manifests as an anomalous aging phenomenon, resulting in a sudden decline in battery capacity, typically characterized by a distinct knee-point on capacity fade curve.

Therefore, the main aging mechanisms contributing to the well-known knee-point on the capacity fade curve include lithium plating at low temperatures and high charging rates, as well as particle cracking and metal dissolution within the electrodes at high temperatures.

In the authors' opinion, although the proposed models in the literature appear to predict the aging behavior of LiBs, in many cases, the aging mechanisms undergo changes. When focusing on cycle aging with batteries cycled at fixed rated currents and SOC ranges, this variation can be observed through the empirical correlation between capacity fade or power fade and cycle time, number of cycles, or moved charge. In the present work, the focus is on capacity fade. Additionally, for a fair comparison, 25 °C can be taken as the reference temperature for non-accelerated aging. For instance, in Ref. [51], the authors conducted tests on LCO batteries, cycling them at three different temperatures (25 °C, 35 °C, and 45 °C) with constant currents of 0.6C and 0.9C. They proposed a model based on the Arrhenius law, where the capacity reduction varies according to temperature and as a function of the number of cycles raised to the power of 0.74 for both currents. They indicated that the proposed model is highly accurate only between 25 °C and 35 °C. However, for temperatures above 35 °C, it deviates, suggesting that a change in the aging mechanism might be the cause, as also reported in Ref. [46]. In any case, at a temperature of 35 °C, they achieved an acceleration factor of about 1.5 compared to 25 °C. Similar results were reported in Ref. [29], where the authors tested NMC batteries at various temperatures ranging from −20 °C to 70 °C, using a constant charge/discharge current of 1C. When considering the capacity fade obtained at 25 °C and 50 °C, it was observed that the aging mechanism changed. However, the acceleration factor was about 1.4. In Ref. [25], the authors conducted different tests on LFP batteries at distinct temperatures (0 °C, 15 °C, 45 °C, and 60 °C) and proposed an aging model for the capacity fade based on the Arrhenius law for temperatures between 15 °C and 60 °C. They excluded the test performed at 0 °C because the trend was completely different. In this case, instead of using the number of cycles, they employed the total moved charge raised to a fixed number, which in turn was a function of the current rate (C/2, 2C, 6C, and 10C) used during cycling. Nevertheless, the exponential term raising the moved charge was approximately fixed at about 0.55 for all current rates. From the results, it is evident that at a temperature of 45 °C and, even more at 60 °C, the experimental data deviated from the empirical relationship, indicating the occurrence of other aging mechanisms. Different results were obtained in Ref. [52], where the authors cycled various LFP batteries at temperatures of 25 °C, 35 °C, 45 °C, and 55 °C, with a constant charge/discharge current of C/3, using an Arrhenius-like behavior relationship as a function of cycle time. They demonstrated that the term elevating the cycle time was 0.5, 0.52, 0.7, and 0.89, respectively. As they stated, for 25 °C and 35 °C, the curves exhibited the same behavior, with the exponential term being approximately 0.5, and the acceleration factor was about 1.5. They suggested that the capacity fade was attributed to SEI growth, while for temperatures of 45 °C and 55 °C, the trend changed due to different aging mechanisms. On the other hand, in Ref. [53], for LFP batteries, the authors performed different cycle aging tests at temperatures of 40 °C, 47.5 °C, and 55 °C, from which they developed an accelerated model later validated at 25 °C. Specifically, considering the capacity fade, the test data performed at 50 °C were not well estimated by the proposed model based on the Arrhenius law. In any case, a comparison between the test conducted at 40 °C and the one at 25 °C revealed an acceleration factor of approximately 2. In all cases, an Arrhenius-like behavior relationship as a function of number of cycles, cycle time, or moved charge was used. It is worth noting that such a function is not able to predict the knee-point after which the capacity fade abruptly accelerates.

It may be interesting to ask whether it is suitable to focus solely on one predominant aging mechanism or to consider the occurrence of multiple aging mechanisms simultaneously, but at different times. In this regard, several studies [17,41,47,54] suggested that lithium plating may occur even under moderate temperatures and charging rates. This phenomenon is attributed to a significant decline in ionic kinetics and loss of active material in graphite electrodes. Furthermore, as stated in the introduction, part of the plated lithium may react with electrolyte, promoting additional SEI growth, which leads to further degradation. This, in turn, exacerbates the occurrence of lithium plating, potentially initiating a cyclic process. This self-reinforcing mechanism was previously documented in Refs. [41,55]. This is a very intriguing observation because it suggests that even when cycling LiBs under favorable temperatures and current rates —where the primary aging mechanism is slow SEI growth—lithium plating may still occur after a certain point. Therefore, the authors believe that it is not only important to identify the dominant aging mechanisms under specific conditions, but also to understand the overall aging path that LiBs experience, even when different aging mechanisms occur at different times or cycling levels. Consequently, an accelerated aging test procedure should be capable of replicating the same aging path of the battery, but in a faster manner.

In any case, we expect that if the battery subjected to accelerated cycle aging tests experiences the same aging mechanisms and follows a similar degradation path as in non-accelerated tests, the normalized capacity trend versus moved charge, number of equivalent full cycles (EFC), or cycle time should align with that of the accelerated tests when the x-axis is scaled by a factor k. This behavior is consistent with the validity of Arrhenius-like models commonly used in the literature, where a change in temperature effectively corresponds to scaling the x-axis by a specific factor. However, from a theoretical perspective, the reverse is not necessarily true. It is possible for different aging mechanisms or degradation paths to result in similar scaled trends. Therefore, to fully validate the aging behavior from a chemical and physical standpoint, post-mortem analysis would be necessary. Nevertheless, since such coincidences are statistically unlikely, we believe that if the proposed analytical model is x-scalable, it is a strong indication that the same aging mechanisms are likely at play, albeit occurring over different time scales.

In light of the above, and as stated in introduction, this study presents a novel accelerated cycle aging test procedure for LCO batteries. This procedure uses temperature as a stress factor to hasten battery degradation related to capacity fade and includes a corresponding analytical model. The chosen temperature range falls within the discussed limits (20–40 °C), where SEI growth can be considered the dominant aging mechanism, particularly in the linear part of the aging curve. Specifically, the proposed test procedure employs a dual-temperature approach, which seeks to evenly stress the two main aging mechanisms—SEI growth and lithium plating—to replicate the same aging path that LiBs would experience under normal aging conditions at the reference temperature of 25 °C. This temperature can be considered the standard room temperature and, as mentioned above, may correspond to the crossover temperature. This approach has the

potential to achieve a theoretical acceleration much greater than that reported in the literature, without altering the battery aging mechanisms compared to what occurs under non-accelerated conditions. Additionally, the proposed cycle aging model is capable of accurately modeling the knee-point in the capacity fade trend. Specifically, two tests were performed on two battery cells of the same type and batch: one using the proposed accelerated cycle aging test and the other using a non-accelerated cycle aging test for comparison.

3. Experimental setup

The battery cells employed for the tests were 10 Ah LCO pouch batteries (8773160 K), manufactured by General Electronics Co. Ltd., with their parameters listed in Table 1.

Tests were performed using a potentiostat (SP-150) connected to a booster (VMP3B-100), both from BioLogic Science Instrument, and controlled by EC-Lab software installed on a PC connected to the devices via Ethernet. Table 2 provides their specifications.

Battery temperature is typically regulated using a climate chamber; however, this approach may result in temperature fluctuations during charge/discharge due to self-heating. To address this issue, the temperature of the battery cells was controlled in an open space using three Peltier cells, placed underneath the battery cell under test and above a heatsink with two fans. The Peltier cells were connected in series between two legs of a full bridge converter (BOOSTXL-DRV8323RX). The current in the Peltier cells was controlled by a microcontroller (F28069M), which acquired measurements from a temperature probe (Pt100) placed on the top side of the battery, compared them with a reference temperature, T_{ref}, and, through a proportional-integral controller and pulse-width modulation, determined the duty cycle for the converter switches. It is worth noting that the battery temperature was measured on the face opposite the Peltier cells. This method is effective because the battery cells are very thin, allowing the temperature to be considered uniform across that dimension. An overview of the test setup is shown in Fig. 2a, while the schematic of the temperature controller is presented in Fig. 2b. Finally, Table 3 reports the specifications for temperature control.

4. Test procedure

As mentioned in the introduction, this work assesses battery degradation in terms of capacity fade. Therefore, the SOH can be defined as follows:

$$\mathrm{SOH} = \frac{C}{C_{in}} \tag{1}$$

where C is the actual battery capacity, i.e., the amount of charge the battery can deliver during discharge, and C_{in} is the capacity of the fresh cell.

To demonstrate that the proposed test procedure effectively accelerates battery aging, two battery cells of the same type were aged: one using the proposed accelerated cycle aging procedure and the other using a non-accelerated cycle aging procedure. In both cases, the procedure was divided into two phases: the characterization phase and the cycle aging phase.

Table 1
Battery specifications.

Rated Capacity	10 Ah
Rated Voltage	3.7 V
Standard Charge Current	0.2C
Max Charge Current	1C
Charge cut-off Voltage	4.2 V
Discharge Current	Continuously: 10C; Max: 15C
Discharge cut-off Voltage	2.75 V
Cell Voltage	3.7–3.9 V
Impedance	≤12 mΩ

Table 2
Potentiostat and booster specifications.

SP-150	
Voltage Range	±10 V
Current Range	±0.8 A
Voltage Measurement Accuracy	<10 mV
Current Measurement Accuracy	<0.8 mA
VMP3B-100	
Voltage Range	0–5 V
Current Range	±100 A
Voltage Measurement Accuracy	<10 mV
Current Measurement Accuracy	1 A
Impedance Measurement Accuracy	1 %,1°

4.1. Characterization phase

The characterization phase aimed to evaluate the capacity of the battery and was identical for both cells. It consisted of a full charge and full discharge performed at 25 °C using the constant current-constant voltage (CC-CV) method. In particular, the battery was first charged with a constant current of 10 A (1C) until the battery voltage reached the maximum cut-off voltage of 4.2 V. Then, the same voltage was applied until the battery current, I_b, dropped below 300 mA (0.03C). At this stage, the battery was considered fully charged, and the discharge phase could start. The battery was then discharged with a constant current of 10 A (1C) until the minimum cut-off voltage of 2.75 V was reached. Following this, the cut-off voltage was maintained until the battery current dropped below 300 mA (0.03C). The capacity, expressed in Ah, was evaluated by integrating the battery current during the discharge phase t_d, as follows:

$$C = \frac{1}{3600}\int_0^{t_d} I_b(\tau)d\tau. \tag{2}$$

4.2. Cycle aging phase

As done in Ref. [23], instead of expressing capacity fade as a function of the number of EFCs, the total moved charge, Q, exchanged with the battery, was used. It is defined as follows:

$$Q = \frac{1}{3600}\int_0^{t} |I_b(\tau)|d\tau. \tag{3}$$

The main idea behind the proposed accelerated cycle aging procedure is to stress the two primary aging mechanisms—SEI growth and lithium plating—in a balanced manner, in order to replicate normal aging tests. As described in the introduction and Section II, when the battery is cycled at temperatures between about 25 °C and 40 °C, SEI growth is the dominant aging mechanism. However, lithium plating also occurs, and the two mechanisms can reinforce each other. This interaction is reflected in the aging curve: the linear part corresponds to SEI growth, while the segment after the knee-point is associated with lithium plating, which is exacerbated by the SEI through a self-reinforcement mechanism. In contrast, cycling the battery—particularly charging it at temperatures lower than 25 °C, which can be considered the crossover temperature—results in lithium plating becoming the dominant aging mechanism.

To achieve this, the accelerated cycle aging procedure involved charging the battery at 20 °C and discharging it at 40 °C. This approach avoided prolonged exposure to both 20 °C and 40 °C, thereby mitigating the aging phenomena associated with these conditions. The decision to discharge the battery at 40 °C was made because this temperature represents the upper limit, beyond which additional aging mechanisms, such as electrolyte dissolution, gas generation, and particle cracking, are

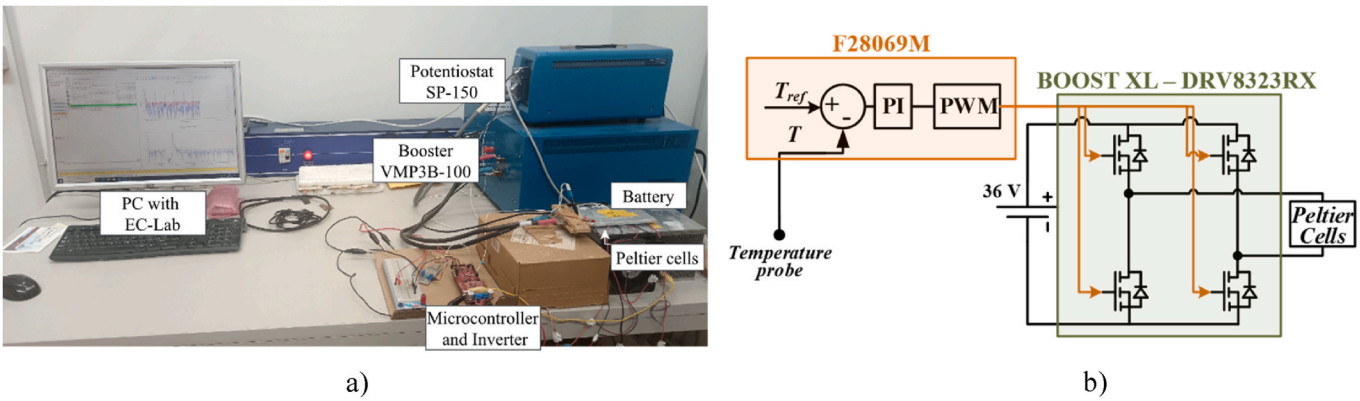

Fig. 2. a) Overview of the test setup; b) Schematic of the temperature controller.

Table 3
Temperature control specifications.

Temperature probe	
Type	WZP Pt100 Platinum resistor
Class	B
Validity range	−20 + 250 °C
Limit deviation	±(0.3 + 0.005·T)
Microcontroller	
Type	F28069M
CPU	C28x 32-Bit Real Time Microcontroller, 90 MHz,
ROM	256 KB Flash
RAM	96 KB
ADC	12-bit
Converter	
Type	BOOSTXL-DRV8323RX
Operating voltage	6 V–54 V
Current	15 A (continuous) 20 A (peak)
Temperature controller	
Type	Closed-loop PI
Response time	8 min
Settling time	15 min
Maximum overshoot	±2 °C

significantly accelerated. Conversely, charging the battery at 20 °C was chosen to induce lithium plating at a rate comparable to that observed at 40 °C. According to Ref. [29], these two temperatures correspond to nearly identical aging rates in the V-shaped Arrhenius law. Thus, discharging the battery at a maximum of 40 °C may primarily accelerate SEI growth, while charging at 20 °C may enhance lithium plating.

This dual-temperature approach may effectively accelerate both aging mechanisms in a balanced manner. More in detail, the procedure was as follows: after the characterization phase, the battery was charged at a constant current of 10 A (1C) until the voltage reached 3 V. The temperature reference was then changed to 20 °C, and the battery was allowed to rest for 15 min until it reached the thermal steady state. Next, the battery was charged at a constant current of 20 A (2C) until the voltage reached 4 V. Once this voltage level was reached, the temperature reference was switched to 40 °C, and the battery rested for another 15 min to achieve thermal steady state. Subsequently, the battery was discharged with a current of 20 A (2C) until the voltage reached 3 V. At this point, the temperature reference was switched back to 20 °C, and after the battery reached thermal steady state, it was charged again at 20 A (2C). This procedure was repeated until the total moved charge during the cycle aging phase, Q_{cy}, reached approximately 500 Ah. Afterwards, a characterization phase was performed again to assess the battery capacity. The temperature was adjusted automatically by the microcontroller, which measured the battery voltage and adjusted the temperature reference accordingly. The voltage and temperature of the battery during one aging phase are reported in Fig. 3a. Additionally, Fig. 3b illustrates the spatial temperature distribution on the top side of the battery under steady-state conditions for both 20 °C and 40 °C.

As shown in Fig. 3a, due to the voltage drop during relaxation times and the different ohmic drop at the two temperatures, the battery was cycled between about 3.2 V and 3.6 V, which corresponds to the low SOC area. Despite varying results in the literature [21], indicates that this SOC range causes the least battery aging for this type of battery. Therefore, we can attribute the accelerated degradation to the different temperatures during charge and discharge phases.

For a fair comparison, the battery undergoing non-accelerated cycle aging should be cycled within the same low SOC range. During the non-accelerated cycle aging, the battery temperature was maintained at a constant reference room temperature of 25 °C. Initially, after the characterization phase, the battery was charged at 10 A (1C), moving 1 Ah, which corresponds to 10 % of its nominal capacity. Subsequently, the battery was discharged at 20 A (2C) until the moved charge reached 0.4 Ah (4 % of the nominal capacity), or the battery voltage dropped to 2.75 V. The battery was then charged again at 20 A (2C) until the moved charge reached 0.4 Ah (4 % of the nominal capacity), or the battery voltage reached 3.65 V. In this way, the battery charge and discharge were limited to a range between −0.4 Ah and 0.4 Ah (±4 % of the nominal capacity), and between 2.75 V and 3.65 V, cycling around a mean SOC of 8 % of the nominal capacity. This procedure was repeated until approximately $Q_{cy} = 1000$ Ah, after which another characterization phase was performed to assess the battery capacity. The testing procedure for both the accelerated and non-accelerated cycles is reported in Fig. 4.

The decision to cycle the battery at a 2C current was made to expedite the testing process without compromising the comparison, as the battery is designed for high-power applications.

5. Experimental results

The capacity results for the battery undergoing non-accelerated cycle aging are reported in Fig. 5a, while the results for the battery undergoing the proposed accelerated cycle aging are presented in Fig. 5b. As seen from the figures, the capacity reduction for $Q = 97$ kAh (4850 EFC) is around 8 % for the non-accelerated test. In contrast, for the accelerated test, the battery experiences a 20 % reduction after less than 4 kAh of moved charge (200 EFC).

However, to determine whether the proposed accelerated procedure accelerates the same aging mechanisms in a consistent manner—without stimulating other mechanisms or altering the proportion of the existing ones—the capacity fade trend should remain consistent. Since in the accelerated test, the capacity reduction exceeded the knee-point (the point after which degradation accelerates abruptly), the fitting procedure was initiated using the results of the accelerated test. Starting with capacity fade expression proposed in Ref. [23], the function was adjusted to accurately reflect the capacity behavior around the

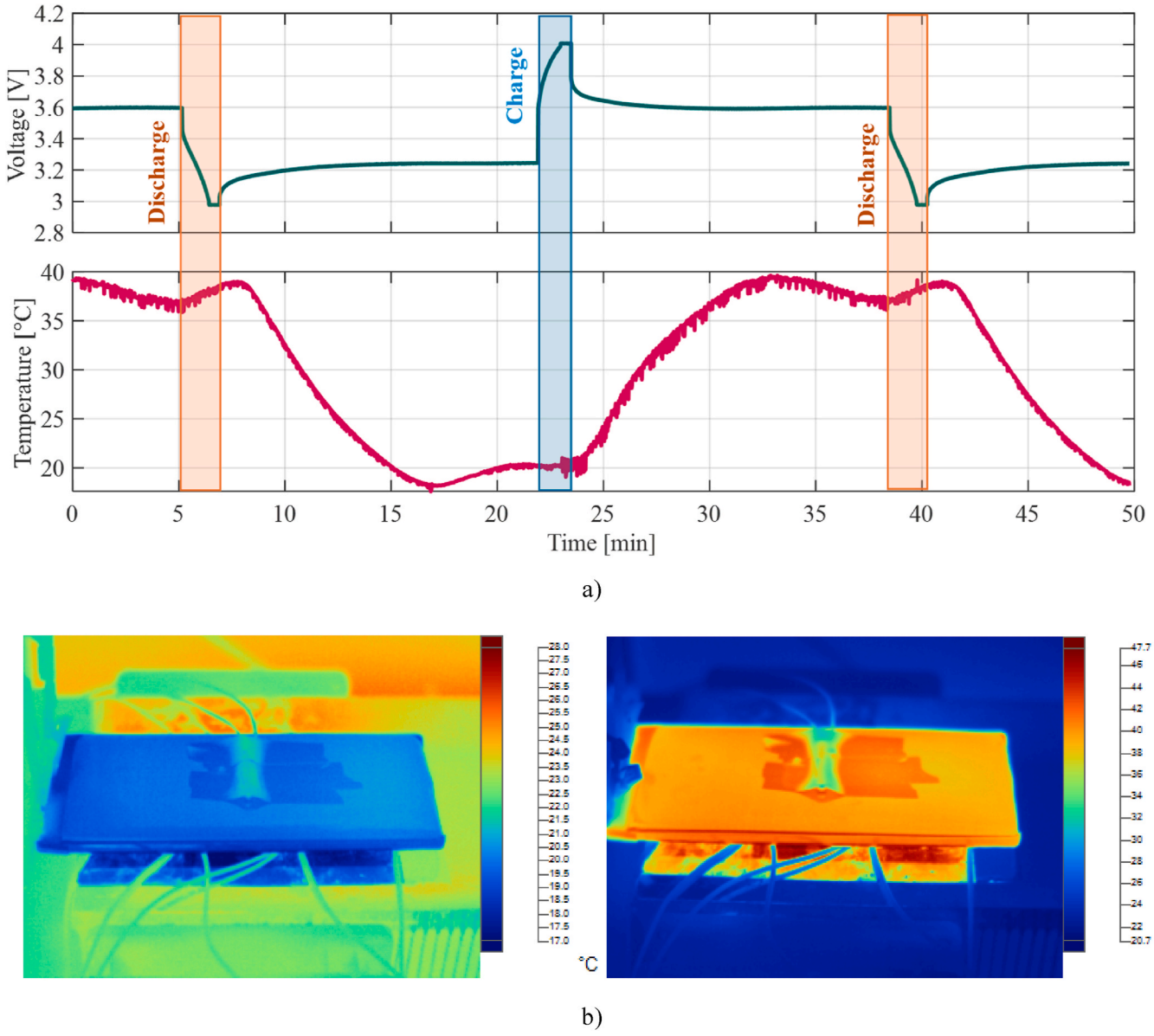

Fig. 3. a) Battery voltage and temperature during the cycle aging phase; b) Spatial temperature distribution on the top side of the battery.

knee-point. The proposed fitting function is:

$$C(Q) = C_i + p_1\sqrt{Q} + p_2 Q + p_3 Q^7. \tag{4}$$

where C_i is the initial capacity of the fitting function, and p_1, p_2, and p_3 are the cycle aging coefficients. It is worth to note that the root and linear terms are the same as those in Ref. [23], while the seventh-degree term replaces the second-degree term of [23].

Using linear least squares minimization, the experimental data from the accelerated test were fitted using (4). Fig. 6a shows the experimental data along with their fitting function, while Table 4 presents the values of the fitting parameters, labeled as $C_{i,a}$, $p_{1,a}$, $p_{2,a}$, and $p_{3,a}$ for the accelerated test. From Fig. 6a, it is evident that the fitting function aligns closely with the experimental data. This result is further supported by the coefficient of determination (R^2), which is 0.9976.

To make the results of the two tests comparable, the battery capacity must be normalized. Instead of using the experimental value of the fresh battery capacity, C_{in}, the normalization was performed with respect to the initial value of the fitting function capacity, $C_{i,a}$. This approach mitigates the uncertainty in the experimental value. Therefore, according to (1), the SOH for the accelerated test is obtained:

$$\mathrm{SOH}_a(Q) = 1 + p_{1,n}\sqrt{Q} + p_{2,n} Q + p_{3,n} Q^7 \tag{5}$$

where $p_{1,n}$, $p_{2,n}$, and $p_{3,n}$, are the normalized cycle aging coefficients, which are reported in Table 5.

Now, considering the results of the non-accelerated cycle aging test and in line with the hypothesis presented in Section II, if the accelerated test truly accelerates the same aging mechanisms in the same manner as the non-accelerated test, then the trend of the normalized capacity with the moved charge (i.e., the SOH of the non-accelerated test) should match the trend of the SOH for the accelerated test when scaled on the x-axis by a factor k:

$$\mathrm{SOH}_{na}(Q) = \mathrm{SOH}_a(k \cdot Q). \tag{6}$$

On the other hand, the normalization factor, $C_{i,na}$, for the non-accelerated test, which represents the initial capacity of the fitting function, must also be found. Therefore, by multiplying the term on the right-hand side of (6) by the factor $C_{i,na}$, the capacity fade for the non-accelerated test can be expressed as follows:

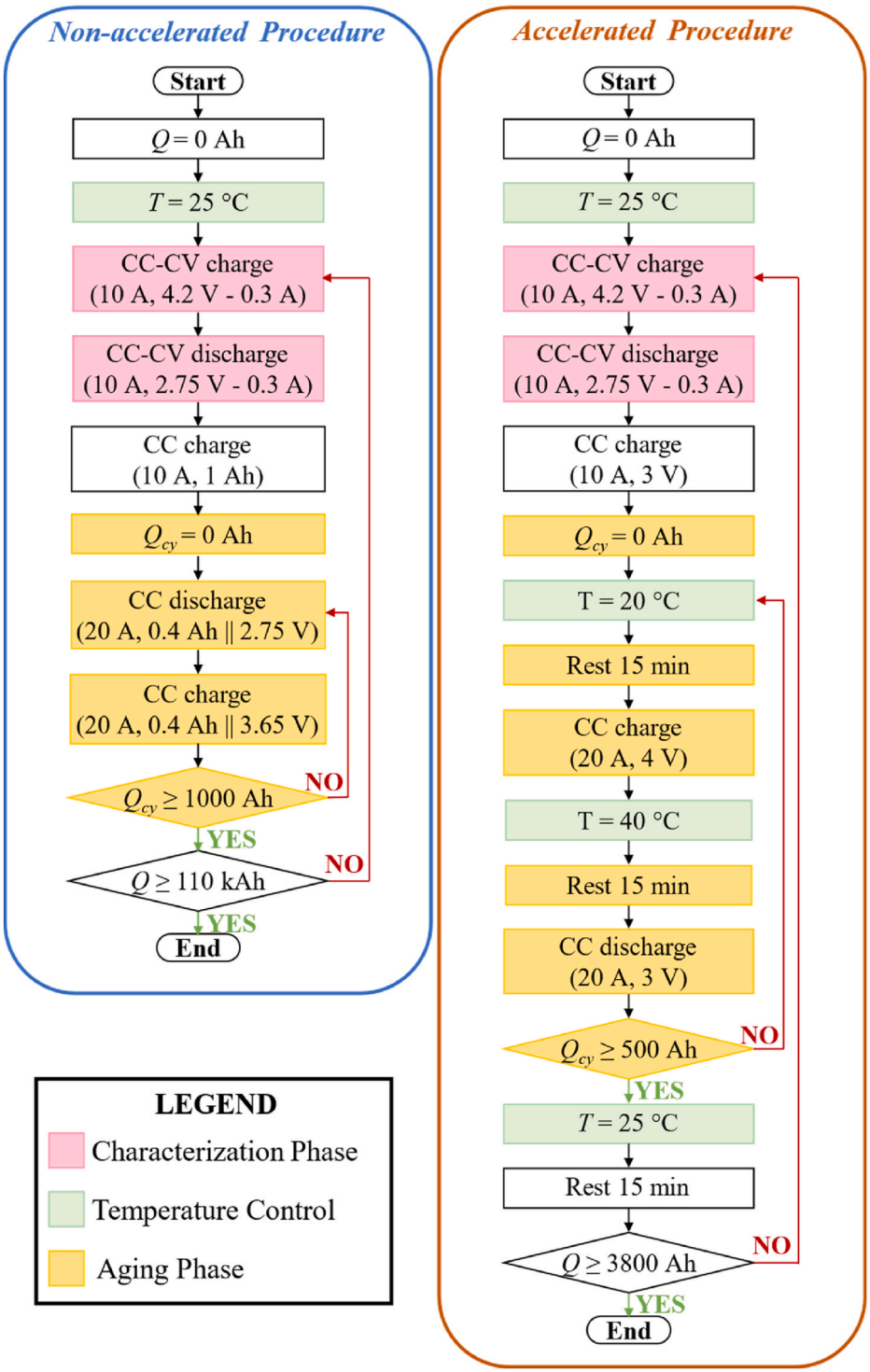

Fig. 4. Test procedure for non-accelerated and accelerated test.

$$C_{na}(Q) = C_{i,na}\left(1 + p_{1,n}\sqrt{k \cdot Q} + p_{2,n}(k \cdot Q) + p_{3,n}(k \cdot Q)^7\right). \quad (7)$$

Therefore, the experimental data of the non-accelerated test were fitted using (7) with nonlinear least squares minimization. The results of this fitting are reported in Fig. 6b, along with the corresponding experimental data. The values of $C_{i,na}$ and k obtained from the fitting are 9.812 and 0.03165, respectively. Similarly, the proposed fitting function provides a good match to the data, with an R^2 value of 0.9846. This indicates that the proposed accelerated cycle aging procedure likely accelerates battery degradation while maintaining the same aging behavior as the non-accelerated test, with an acceleration factor equal to $1/k$.

Finally, the data from the non-accelerated test can also be normalized using the initial value of the corresponding fitting function. The results of the two normalized capacities, along with their respective fitting functions, are shown in Fig. 7.

According to the acceleration factor, the proposed procedure theoretically accelerates degradation by about 30 times. However, this estimation holds true solely when considering the difference in Ah moved to achieve the same capacity fade. When accounting for time as

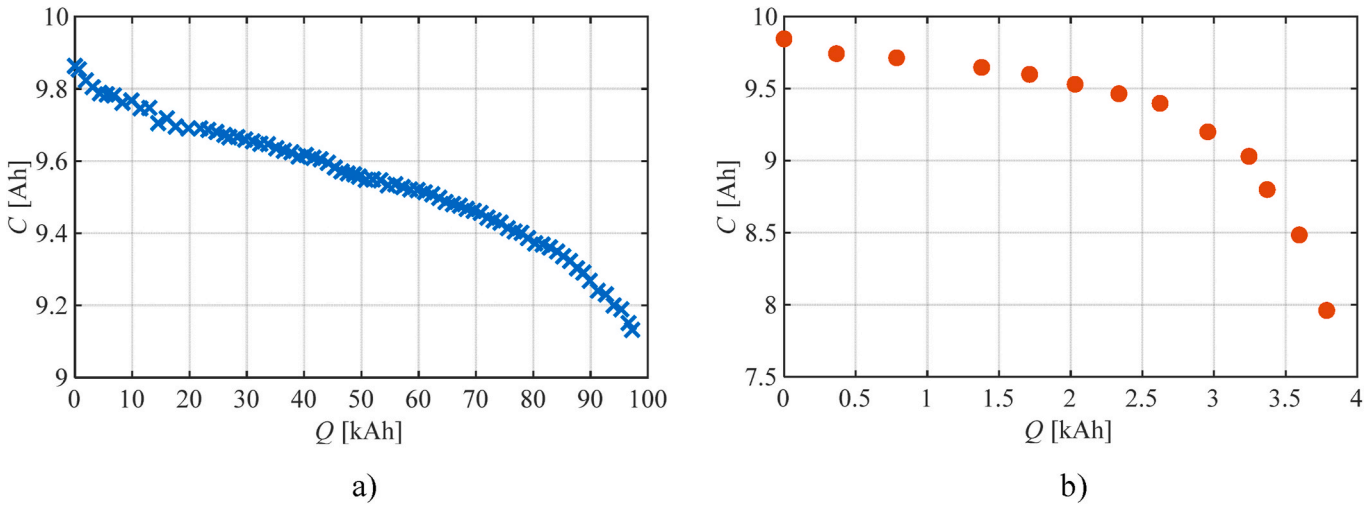

Fig. 5. Results of the capacity fade for: a) non-accelerated cycle aging test; b) accelerated cycle aging test.

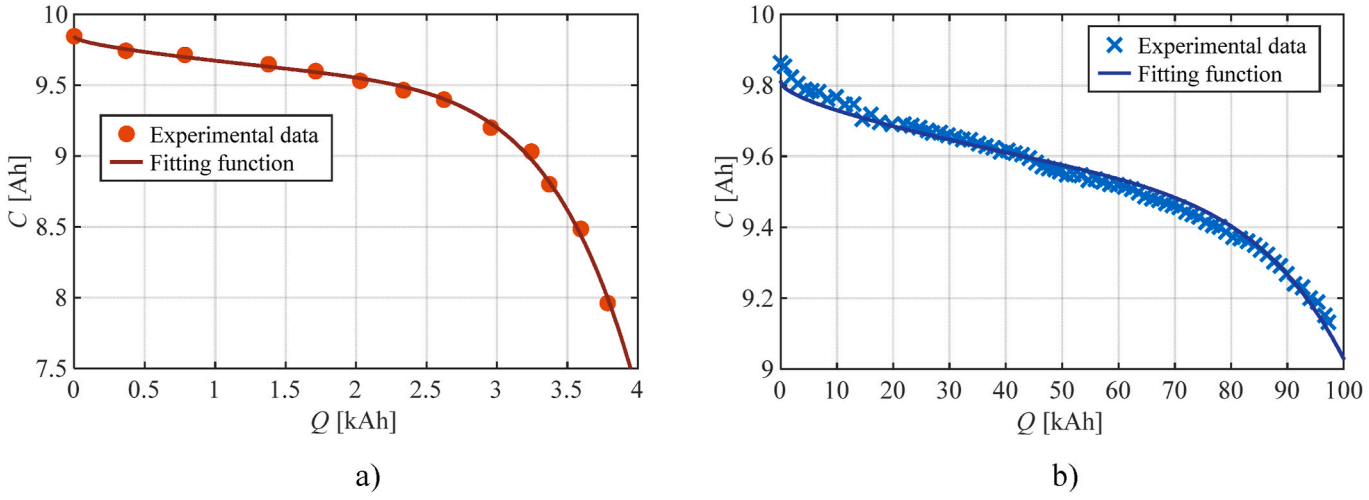

Fig. 6. Results of the capacity fade for: a) accelerated test with fitting function; b) non-accelerated test with fitting function.

an indicator, the duration for transitioning between temperatures (from 20 °C to 40 °C and vice versa) is limited to 15 min due to constraints in the test setup's heating and cooling capabilities. Consequently, approximately 1200 h are required to reach 80 % of the initial capacity.

Examining the fitting function of the non-accelerated test reveals that reaching an 80 % capacity loss corresponds to moving approximately 121 kAh. This implies a total time of about 6050 h, assuming continuous operation and cycling at a current of 20 A. From a temporal standpoint, this suggests that the proposed procedure accelerates degradation by approximately 5 times, representing a significant improvement compared to results reported in the literature. However, with a more efficient test setup capable of achieving temperature steady states in 8 min instead of 15, the total time required could potentially be reduced to 700 h. This improvement would further accelerate degradation by more than 8 times compared to the current setup. Finally, Fig. 8 displays the fitting function of the SOH of the non-accelerated test, alongside its experimental data, as well as the results of the accelerated test scaled on the x-axis by the acceleration factor $1/k$. As shown, the

Table 4
Fitting parameters of the accelerated cycle aging test.

$C_{i,a}$ [Ah]	$p_{1,a}$ [Ah$^{1/2}$]	$p_{2,a}$	$p_{3,a}$ [Ah^{-6}]
9.845	$-3.690{\cdot}10^{-3}$	$-5.565{\cdot}10^{-5}$	$-1.266{\cdot}10^{-25}$

Table 5
Normalized fitting parameters of the accelerated cycle aging test.

$p_{1,n}$ [Ah$^{1/2}$]	$p_{2,n}$	$p_{3,n}$ [Ah^{-6}]
$-3.748{\cdot}10^{-4}$	$-5.652{\cdot}10^{-6}$	$-1.286{\cdot}10^{-26}$

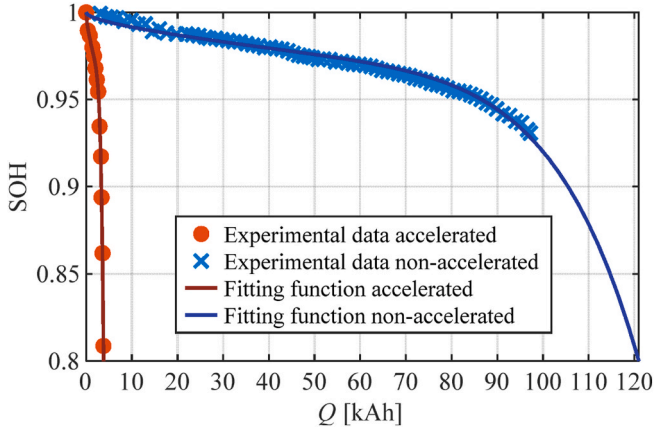

Fig. 7. Normalized capacity (SOH) results.

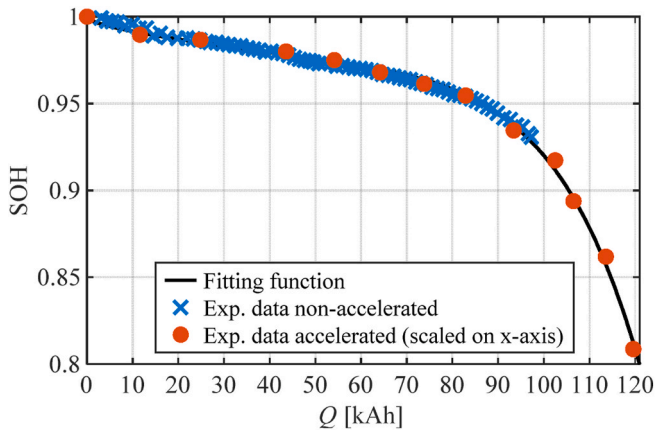

Fig. 8. Results of the non-accelerated cycle aging test and accelerated cycle aging test scaled on x-axis.

two curves overlap almost perfectly.

6. Conclusion

This study proposed and validated a novel accelerated cycle aging test procedure focusing on capacity fade, based on a dual-temperature approach that uses battery temperature as a stress factor. Unlike previous literature, which typically achieves an acceleration factor of less than 2 by considering temperatures of 35–50 °C with respect to 25 °C, or by altering battery aging mechanisms, the proposed method aims to achieve a significantly higher acceleration factor than those reported in the literature while preserving the original aging path observed under normal conditions.

The proposed accelerated cycle aging method assumes that under typical operational temperatures between 20 °C and 40 °C, the primary aging mechanisms are SEI growth during the linear phase of capacity fade, with both SEI growth and lithium plating occurring after the knee-point, where self-reinforcement takes place. By charging the battery at 20 °C and discharging it at 40 °C, we aim to consistently accelerate these mechanisms in a way that reflects the non-accelerated aging process.

Analytically, this implies that the accelerated capacity fade trend should closely align with the non-accelerated trend when the x-axis, representing the moved charge, is properly scaled by the acceleration factor. The reported results demonstrate that achieving an acceleration factor approximately 5 times higher than the non-accelerated test is feasible. Furthermore, with enhancements to the heating/cooling system, an acceleration factor greater than 8 could potentially be achieved.

These findings represent significant advancements compared to existing literature, promising accelerated aging factors that can ensure the preservation of consistent aging mechanisms throughout the accelerated testing process. Moreover, the proposed accelerated cycle aging procedure requires only a simple temperature control system capable of heating or cooling the battery under test. Specifically, a low-cost hardware setup was employed, consisting of an F28069M microcontroller paired with the BOOSTXL-DRV8323RX converter, both manufactured by Texas Instruments, along with a Pt100 temperature probe.

Although the proposed accelerated cycle aging procedure was conducted on an LCO battery, different battery chemistries may result in varying crossover temperatures at which SEI growth or lithium plating becomes the dominant aging mechanism. However, in the authors' opinion, cobalt-based lithium-ion batteries, such as NMC and NCA, may exhibit similar behaviors, allowing for the use of the same charging and discharging temperatures. For chemistries like LFP, different temperature values may be required, although the overall methodology would remain applicable. Extending the proposed accelerated cycle aging procedure to other battery chemistries is planned for future research.

CRediT authorship contribution statement

Simone Barcellona: Writing – review & editing, Writing – original draft, Validation, Methodology, Formal analysis, Conceptualization. **Silvia Colnago:** Writing – review & editing, Writing – original draft, Validation, Methodology, Formal analysis, Conceptualization. **Lorenzo Codecasa:** Writing – review & editing, Supervision. **Luigi Piegari:** Writing – review & editing, Supervision, Methodology, Formal analysis, Conceptualization.

Declaration of competing interest

The authors declare that they have no known competing financial interests or personal relationships that could have appeared to influence the work reported in this paper.

Acknowledgements

This work has been partially financed by the Research Fund for the Italian Electrical System under the Three-Year Research Plan 2025–2027 (DM MASE n. 388, November 06, 2024), in compliance with the Decree of April 12th, 2024.

Appendix A. Supplementary data

Supplementary data to this article can be found online at https://doi.org/10.1016/j.jpowsour.2025.237167.

Data availability

The authors are unable or have chosen not to specify which data has been used.

References

[1] M.A. Divakaran, M. Minakshi, P.A. Bahri, S. Paul, P. Kumari, A.M. Divakaran, K. N. Manjunatha, Rational design on materials for developing next generation lithium-ion secondary battery, Prog. Solid State Chem. 62 (2021) 100298, https://doi.org/10.1016/j.progsolidstchem.2020.100298.

[2] M.A. Hannan, S.B. Wali, P.J. Ker, M.S.A. Rahman, M. Mansor, V. K. Ramachandaramurthy, K.M. Muttaqi, T.M.I. Mahlia, Z.Y. Dong, Battery energy-storage system: a review of technologies, optimization objectives, constraints, approaches, and outstanding issues, J. Energy Storage 42 (2021) 103023, https://doi.org/10.1016/j.est.2021.103023.

[3] V.S.K. Sungjemmenla, C.B. Soni, V. Kumar, Z.W. Seh, Understanding the cathode–electrolyte interphase in lithium-ion batteries, Energy Technol. 10 (2022), https://doi.org/10.1002/ente.202200421.

[4] S.B. Chikkannanavar, D.M. Bernardi, L. Liu, A review of blended cathode materials for use in Li-ion batteries, J. Power Sources 248 (2014) 91–100, https://doi.org/10.1016/j.jpowsour.2013.09.052.

[5] H. Zhu, J. Ma, H. Ding, H. Wu, C. Zhang, L. Ni, X. Fang, L. Lao, X. Wang, A novel multifunctional electrolyte system for high performance Li-ion batteries, Appl. Surf. Sci. 677 (2024) 161100, https://doi.org/10.1016/j.apsusc.2024.161100.

[6] R. Li, L. Bao, L. Chen, C. Zha, J. Dong, N. Qi, R. Tang, Y. Lu, M. Wang, R. Huang, K. Yan, Y. Su, F. Wu, Accelerated aging of lithium-ion batteries: bridging battery aging analysis and operational lifetime prediction, Sci. Bull. 68 (2023) 3055–3079, https://doi.org/10.1016/j.scib.2023.10.029.

[7] X. Lin, K. Khosravinia, X. Hu, J. Li, W. Lu, Lithium plating mechanism, detection, and mitigation in lithium-ion batteries, Prog. Energy Combust. Sci. 87 (2021) 100953, https://doi.org/10.1016/j.pecs.2021.100953.

[8] Q. Liu, C. Du, B. Shen, P. Zuo, X. Cheng, Y. Ma, G. Yin, Y. Gao, Understanding undesirable anode lithium plating issues in lithium-ion batteries, RSC Adv. 6 (2016) 88683–88700, https://doi.org/10.1039/C6RA19482F.

[9] A. Barré, B. Deguilhem, S. Grolleau, M. Gérard, F. Suard, D. Riu, A review on lithium-ion battery ageing mechanisms and estimations for automotive applications, J. Power Sources 241 (2013) 680–689, https://doi.org/10.1016/j.jpowsour.2013.05.040.

[10] M. Fan, X. Chang, X.-H. Meng, C.-F. Gu, C.-H. Zhang, Q. Meng, L.-J. Wan, Y.-G. Guo, Structural restoration of degraded LiFePO 4 cathode with enhanced kinetics using residual lithium in spent graphite anodes, CCS Chem. 5 (2023) 1189–1201, https://doi.org/10.31635/ccschem.022.202201996.

[11] G. Kucinskis, M. Bozorgchenani, M. Feinauer, M. Kasper, M. Wohlfahrt-Mehrens, T. Waldmann, Arrhenius plots for Li-ion battery ageing as a function of temperature, C-rate, and ageing state – an experimental study, J. Power Sources 549 (2022) 232129, https://doi.org/10.1016/j.jpowsour.2022.232129.

[12] M. Ecker, J.B. Gerschler, J. Vogel, S. Käbitz, F. Hust, P. Dechent, D.U. Sauer, Development of a lifetime prediction model for lithium-ion batteries based on extended accelerated aging test data, J. Power Sources 215 (2012) 248–257, https://doi.org/10.1016/j.jpowsour.2012.05.012.
[13] J. Schmalstieg, S. Kabitz, M. Ecker, D.U. Sauer, From accelerated aging tests to a lifetime prediction model: analyzing lithium-ion batteries, in: 2013 World Electr. Veh. Symp. Exhib., IEEE, 2013, pp. 1–12, https://doi.org/10.1109/EVS.2013.6914753.
[14] Y. Gao, J. Jiang, C. Zhang, W. Zhang, Y. Jiang, Aging mechanisms under different state-of-charge ranges and the multi-indicators system of state-of-health for lithium-ion battery with Li(NiMnCo)O2 cathode, J. Power Sources 400 (2018) 641–651, https://doi.org/10.1016/j.jpowsour.2018.07.018.
[15] Y. Zhu, F. Yan, J. Kang, C. Du, C. Zhang, R.F. Turkson, Fading analysis of the Li (NiCoMn)O2 battery under different SOC cycle intervals, Ionics (Kiel) 23 (2017) 1383–1390, https://doi.org/10.1007/s11581-016-1968-7.
[16] E. Wikner, E. Björklund, J. Fridner, D. Brandell, T. Thiringer, How the utilised SOC window in commercial Li-ion pouch cells influence battery ageing, J. Power Sources Adv. 8 (2021) 100054, https://doi.org/10.1016/j.powera.2021.100054.
[17] M. Ecker, N. Nieto, S. Käbitz, J. Schmalstieg, H. Blanke, A. Warnecke, D.U. Sauer, Calendar and cycle life study of Li(NiMnCo)O2-based 18650 lithium-ion batteries, J. Power Sources 248 (2014) 839–851, https://doi.org/10.1016/j.jpowsour.2013.09.143.
[18] J. Zhu, M. Knapp, D.R. Sørensen, M. Heere, M.S.D. Darma, M. Müller, L. Mereacre, H. Dai, A. Senyshyn, X. Wei, H. Ehrenberg, Investigation of capacity fade for 18650-type lithium-ion batteries cycled in different state of charge (SoC) ranges, J. Power Sources 489 (2021) 229422, https://doi.org/10.1016/j.jpowsour.2020.229422.
[19] S. Gantenbein, M. Schönleber, M. Weiss, E. Ivers-Tiffée, Capacity fade in lithium-ion batteries and cyclic aging over various State-of-Charge ranges, Sustainability 11 (2019) 6697, https://doi.org/10.3390/su11236697.
[20] W. Wang, B. Yuan, Q. Sun, R. Wennersten, Analysis and modeling of calendar aging and cycle aging of LiCoO2/Graphite cells, J. Therm. Sci. (2024), https://doi.org/10.1007/s11630-024-1918-z.
[21] S. Barcellona, L. Codecasa, S. Colnago, L. Piegari, Open-circuit voltage variation in LiCoO2 battery cycled in different states of charge regions, Energies 17 (2024) 2364, https://doi.org/10.3390/en17102364.
[22] W. Diao, S. Saxena, M. Pecht, Accelerated cycle life testing and capacity degradation modeling of LiCoO2-graphite cells, J. Power Sources 435 (2019) 226830, https://doi.org/10.1016/j.jpowsour.2019.226830.
[23] S. Barcellona, L. Piegari, Effect of current on cycle aging of lithium ion batteries, J. Energy Storage 29 (2020) 101310, https://doi.org/10.1016/j.est.2020.101310.
[24] G. Ning, B. Haran, B.N. Popov, Capacity fade study of lithium-ion batteries cycled at high discharge rates, J. Power Sources 117 (2003) 160–169, https://doi.org/10.1016/S0378-7753(03)00029-6.
[25] J. Wang, P. Liu, J. Hicks-Garner, E. Sherman, S. Soukiazian, M. Verbrugge, H. Tataria, J. Musser, P. Finamore, Cycle-life model for graphite-LiFePO4 cells, J. Power Sources 196 (2011) 3942–3948, https://doi.org/10.1016/j.jpowsour.2010.11.134.
[26] N. Omar, M.A. Monem, Y. Firouz, J. Salminen, J. Smekens, O. Hegazy, H. Gaulous, G. Mulder, P. Van den Bossche, T. Coosemans, J. Van Mierlo, Lithium iron phosphate based battery – assessment of the aging parameters and development of cycle life model, Appl. Energy 113 (2014) 1575–1585, https://doi.org/10.1016/j.apenergy.2013.09.003.
[27] T. Waldmann, M. Kasper, M. Wohlfahrt-Mehrens, Optimization of charging strategy by prevention of lithium deposition on anodes in high-energy lithium-ion batteries – electrochemical experiments, Electrochim. Acta 178 (2015) 525–532, https://doi.org/10.1016/j.electacta.2015.08.056.
[28] Y. Preger, H.M. Barkholtz, A. Fresquez, D.L. Campbell, B.W. Juba, J. Romàn-Kustas, S.R. Ferreira, B. Chalamala, Degradation of commercial lithium-ion cells as a function of chemistry and cycling conditions, J. Electrochem. Soc. 167 (2020) 120532, https://doi.org/10.1149/1945-7111/abae37.
[29] T. Waldmann, M. Wilka, M. Kasper, M. Fleischhammer, M. Wohlfahrt-Mehrens, Temperature dependent ageing mechanisms in Lithium-ion batteries – a post-mortem study, J. Power Sources 262 (2014) 129–135, https://doi.org/10.1016/j.jpowsour.2014.03.112.
[30] I. Bloom, B. Cole, J. Sohn, S. Jones, E. Polzin, V. Battaglia, G. Henriksen, C. Motloch, R. Richardson, T. Unkelhaeuser, D. Ingersoll, H. Case, An accelerated calendar and cycle life study of Li-ion cells, J. Power Sources 101 (2001) 238–247, https://doi.org/10.1016/S0378-7753(01)00783-2.
[31] R. Spotnitz, Simulation of capacity fade in lithium-ion batteries, J. Power Sources 113 (2003) 72–80, https://doi.org/10.1016/S0378-7753(02)00490-1.
[32] B.Y. Liaw, E.P. Roth, R.G. Jungst, G. Nagasubramanian, H.L. Case, D.H. Doughty, Correlation of arrhenius behaviors in power and capacity fades with cell impedance and heat generation in cylindrical lithium-ion cells, J. Power Sources 119–121 (2003) 874–886, https://doi.org/10.1016/S0378-7753(03)00196-4.
[33] R. Deshpande, M. Verbrugge, Y.-T. Cheng, J. Wang, P. Liu, Battery cycle life prediction with coupled chemical degradation and fatigue mechanics, J. Electrochem. Soc. 159 (2012) A1730–A1738, https://doi.org/10.1149/2.049210jes.
[34] S. Shahid, M. Agelin-Chaab, A review of thermal runaway prevention and mitigation strategies for lithium-ion batteries, Energy Convers. Manag. X 16 (2022) 100310, https://doi.org/10.1016/j.ecmx.2022.100310.
[35] T. Gewald, M. Lienkamp, A systematic method for accelerated aging characterization of lithium-ion cells in automotive applications, Forsch. Im. Ingenieurwes. 83 (2019) 831–841, https://doi.org/10.1007/s10010-019-00318-9.
[36] J. Liang, Y. Gan, M. Yao, Y. Li, Numerical analysis of capacity fading for a LiFePO4 battery under different current rates and ambient temperatures, Int. J. Heat Mass Tran. 165 (2021) 120615, https://doi.org/10.1016/j.ijheatmasstransfer.2020.120615.
[37] Y. Li, K. Li, W. Shen, J. Huang, X. Qu, Y. Zhang, Y. Lin, Stress-dependent capacity fade behavior and mechanism of lithium-ion batteries, J. Energy Storage 86 (2024) 111165, https://doi.org/10.1016/j.est.2024.111165.
[38] H. Zhu, J. Ma, H. Ding, H. Wu, C. Zhang, X. Fang, H. Xuan, L. Lao, L. Ni, X. Wang, Experimental study of capacity fading mechanism in multiple overdischarge on LiNi0.5Co0.2Mn0.3O2& LiMn2O4/graphite lithium-ion batteries, Ceram. Int. 50 (2024) 35537–35548, https://doi.org/10.1016/j.ceramint.2024.06.366.
[39] R. Wright, J. Christophersen, C. Motloch, J. Belt, C. Ho, V. Battaglia, J. Barnes, T. Duong, R. Sutula, Power fade and capacity fade resulting from cycle-life testing of advanced technology development program lithium-ion batteries, J. Power Sources 119–121 (2003) 865–869, https://doi.org/10.1016/S0378-7753(03)00190-3.
[40] R. Wright, C. Motloch, J. Belt, J. Christophersen, C. Ho, R. Richardson, I. Bloom, S. Jones, V. Battaglia, G. Henriksen, T. Unkelhaeuser, D. Ingersoll, H. Case, S. Rogers, R. Sutula, Calendar- and cycle-life studies of advanced technology development program generation 1 lithium-ion batteries, J. Power Sources 110 (2002) 445–470, https://doi.org/10.1016/S0378-7753(02)00210-0.
[41] M. Broussely, P. Biensan, F. Bonhomme, P. Blanchard, S. Herreyre, K. Nechev, R. J. Staniewicz, Main aging mechanisms in li ion batteries, J. Power Sources 146 (2005) 90–96, https://doi.org/10.1016/j.jpowsour.2005.03.172.
[42] M. Börner, A. Friesen, M. Grützke, Y.P. Stenzel, G. Brunklaus, J. Haetge, S. Nowak, F.M. Schappacher, M. Winter, Correlation of aging and thermal stability of commercial 18650-type lithium ion batteries, J. Power Sources 342 (2017) 382–392, https://doi.org/10.1016/j.jpowsour.2016.12.041.
[43] T.M. Bandhauer, S. Garimella, T.F. Fuller, A critical review of thermal issues in lithium-ion batteries, J. Electrochem. Soc. 158 (2011) R1, https://doi.org/10.1149/1.3515880.
[44] D. Mazouzi, Z. Karkar, C. Reale Hernandez, P. Jimenez Manero, D. Guyomard, L. Roué, B. Lestriez, Critical roles of binders and formulation at multiscales of silicon-based composite electrodes, J. Power Sources 280 (2015) 533–549, https://doi.org/10.1016/j.jpowsour.2015.01.140.
[45] T. Wang, Y. Zhu, W. Zhao, Y. Gong, Z. Zhang, W. Gao, Y. Shang, Capacity degradation analysis and knee point prediction for lithium-ion batteries, Green Energy Intell. Transp. (2024) 100171, https://doi.org/10.1016/j.geits.2024.100171.
[46] J.C. Burns, A. Kassam, N.N. Sinha, L.E. Downie, L. Solnickova, B.M. Way, J. R. Dahn, Predicting and extending the lifetime of Li-Ion batteries, J. Electrochem. Soc. 160 (2013) A1451–A1456, https://doi.org/10.1149/2.060309jes.
[47] M. Klett, R. Eriksson, J. Groot, P. Svens, K. Ciosek Högström, R.W. Lindström, H. Berg, T. Gustafson, G. Lindbergh, K. Edström, Non-uniform aging of cycled commercial LiFePO4//graphite cylindrical cells revealed by post-mortem analysis, J. Power Sources 257 (2014) 126–137, https://doi.org/10.1016/j.jpowsour.2014.01.105.
[48] J. Wang, J. Purewal, P. Liu, J. Hicks-Garner, S. Soukazian, E. Sherman, A. Sorenson, L. Vu, H. Tataria, M.W. Verbrugge, Degradation of lithium ion batteries employing graphite negatives and nickel–cobalt–manganese oxide + spinel manganese oxide positives: part 1, aging mechanisms and life estimation, J. Power Sources 269 (2014) 937–948, https://doi.org/10.1016/j.jpowsour.2014.07.030.
[49] M. Ouyang, Z. Chu, L. Lu, J. Li, X. Han, X. Feng, G. Liu, Low temperature aging mechanism identification and lithium deposition in a large format Lithium iron phosphate battery for different charge profiles, J. Power Sources 286 (2015) 309–320, https://doi.org/10.1016/j.jpowsour.2015.03.178.
[50] T. Baumhöfer, M. Brühl, S. Rothgang, D.U. Sauer, Production caused variation in capacity aging trend and correlation to initial cell performance, J. Power Sources 247 (2014) 332–338, https://doi.org/10.1016/j.jpowsour.2013.08.108.
[51] Y. Cui, C. Du, G. Yin, Y. Gao, L. Zhang, T. Guan, L. Yang, F. Wang, Multi-stress factor model for cycle lifetime prediction of lithium ion batteries with shallow-depth discharge, J. Power Sources 279 (2015) 123–132, https://doi.org/10.1016/j.jpowsour.2015.01.003.
[52] S. Sun, T. Guan, B. Shen, K. Leng, Y. Gao, X. Cheng, G. Yin, Changes of degradation mechanisms of LiFePO4/Graphite batteries cycled at different ambient temperatures, Electrochim. Acta 237 (2017) 248–258, https://doi.org/10.1016/j.electacta.2017.03.158.
[53] D.-I. Stroe, M. Swierczynski, A.-I. Stan, R. Teodorescu, S.J. Andreasen, Accelerated lifetime testing methodology for lifetime estimation of lithium-ion batteries used in augmented wind power plants, IEEE Trans. Ind. Appl. 50 (2014) 4006–4017, https://doi.org/10.1109/TIA.2014.2321028.
[54] E. Sarasketa-Zabala, F. Aguesse, I. Villarreal, L.M. Rodriguez-Martinez, C.M. López, P. Kubiak, Understanding lithium inventory loss and sudden performance fade in cylindrical cells during cycling with deep-discharge steps, J. Phys. Chem. C 119 (2015) 896–906, https://doi.org/10.1021/jp510071d.
[55] M. Petzl, M. Kasper, M.A. Danzer, Lithium plating in a commercial lithium-ion battery – a low-temperature aging study, J. Power Sources 275 (2015) 799–807, https://doi.org/10.1016/j.jpowsour.2014.11.065.